# Migrating Thermal Structure in a Freshwater Thermocline

JOHN LAZIER AND HELMUTH SANDSTROM

*Bedford Institute of Oceanography, Dartmouth, Nova Scotia, B2Y 4A2 Canada*

(Manuscript received 4 November 1977, in final form 11 May 1978)

ABSTRACT

The vertical migration of thermal structure in freshwater thermoclines is investigated with theory and observations. The theory is for the wind-forced internal oscillations of a viscous, nonrotating, long narrow lake of constant stratification. The introduction of viscosity results in a smooth phase change with depth near the nodes of the vertical displacement profiles. The gradual change of phase enables the theory to model the observed vertical migration of the temperature structure created by the internal oscillations. The theory is compared to data obtained from a vertical array of thermistors moored in a stratified freshwater lake. Vertical phase profiles calculated from the thermistor chain data agree well with the theoretical profiles for values of kinematic viscosity of about $10.0 \times 10^{-6}$ m$^2$s$^{-1}$. The amplitudes of the vertical displacement away from the nodes agree reasonably well with values predicted by the theory. The agreement is sufficient to warrant the description of the migrating structures in terms of damped internal oscillations of the lake.

## 1. Introduction

Some years ago, Lazier (1973) obtained a series of 61 temperature-depth profiles in Lake Bala in Northern Wales, which demonstrated that some of the thermal structures in a freshwater thermocline migrate vertically through the water column with time. In that paper it was shown that simple internal waves cause structures, and that the migrating property is due to the phase progression of the wave. The internal wave was visualized as originating from a bathymetric irregularity. The free internal oscillation, the internal seiche, of the lake would cause water to flow back and forth across the irregularity, thereby producing an internal wave in just the opposite sense that the oscillator in the experiments of Mowbray and Rarity (1967) creates internal waves. The energy of the internal wave so created would propagate away from the bathymetric bumps in the same way that it does from the oscillator in the experimental tank. Because the particle motion associated with the wave is inclined to the horizontal, the temperature field within the limits of the internal wave beam would be distorted, and a piece of structure would be evident in a vertical profile through the beam. The structure would appear to migrate across the beam with the advance of phase in the internal wave. This idea applied to the profiles from Lake Bala has a major flaw. The energy of the internal wave beam exists only between well-defined limits fixed by the size of the oscillator (Turner, 1973, p. 24). Thus the deformation of the density field, or the structure, cannot exist outside the internal wave beam and the structure cannot migrate through the boundaries of the beam. Examination of the data, however, showed that some structures migrated further in the vertical direction than would be consistent with such a constraint. Another difficulty is that the motion within the internal wave beam must exist along with the background internal seiche motion which is the generator of the internal wave beam. This also was not observed. Upon examination of the data, it was seen that the temperature variations that take part in creating the structure are also associated with the internal seiche oscillation. Thus, understanding migrating structure became a problem of understanding the nature of the internal oscillations of the lake.

The period of the oscillations giving rise to the structures in Lake Bala appeared to be about the same as the record length, i.e., 10 h. Much longer records were obviously necessary to describe the low-frequency oscillations; these were subsequently obtained in Lake William, Nova Scotia, during the summers of 1973 and 1975. A full description of these data is contained in Lazier (1977). The data consist of temperature-depth profiles, similar to those obtained in Lake Bala, and temperature time series at various levels in the lake obtained with thermistor chains. Both types of data from Lake William confirm the existence of migrating structure and strengthen the conviction that the phenomenon is an effect of the internal oscillations of the lake.

The purpose of this paper is to present a linear theory for the forced internal oscillations in a

0022-3670/78/1070-1079$05.00

viscous stratified lake, and to demonstrate by comparison with some of the Lake William data that the theory provides a satisfactory model of the migrating structure phenomenon.

## 2. Theory

Systematic studies of internal oscillations of freshwater lakes began with some observations of temperature fluctuations in Loch Ness by Watson (1904), who interpreted them as standing interfacial waves and found fair agreement between observed and calculated periods. Wedderburn (1912) made many temperature measurements in Loch Earn and confirmed the existence of the internal seiche. He also demonstrated a positive connection between surface wind and the interior oscillation.

These studies and later works, for example, by Mortimer (1952), Proudman (1953, p. 360) and Heaps (1960) were mainly concerned with the determination of the internal seiche periods and modes under various assumptions as to the vertical structure of temperature. Depending on whether the model contained two layers, three layers or a continuous density distribution, two, three or many internal seiche modes could be present.

Although vertical standing waves cause distortions in the vertical density profile, there is no vertical migration of the distortions because there is no vertical phase progression in the standing waves. The perfect standing wave rarely occurs in nature, however, since the two progressive components, of which it is formed, are usually of different amplitudes. The two unequal components can be resolved into standing and progressive waves, and it can be shown that the structure migration is caused by the progressive component.

The theoretical model proposed here is an extension of Proudman's (1953) theory with continuous stratification to include dissipation, which is responsible for the formation of the imperfect standing waves. The model also includes external forcing, but is different in this respect from Lazier's (1973) proposition since the generator of the internal waves lies in the surface layer rather than at a bump in the bathymetry. The structure-forming oscillations are part of the forced response of the lake and hence part of the system of internal seiches rather than something derived from the seiche. The analysis, therefore, is for the forced oscillations of a long, narrow, nonrotating body of viscous fluid with constant stratification.

The origin of the coordinate system is at one end of the lake and in the level bottom. The lake has length $L$ and depth $h$. The wind forcing at the surface ($z = h$) is assumed to be periodic with frequency $\sigma$. The bottom friction is taken to be proportional to the tangential velocity and the basic state of the fluid is taken to be one of no motion with a vertical density distribution given by $\rho_0(z)$. The linearized equations of motion, incompressibility and continuity for the perturbed fields are

$$\rho_0(z)\left(\frac{\partial u}{\partial t} - \nu\frac{\partial^2 u}{\partial z^2}\right) = -\frac{\partial p}{\partial x}, \tag{1}$$

$$\frac{\partial p}{\partial z} + g\rho' = 0, \tag{2}$$

$$\frac{\partial \rho'}{\partial t} + w\frac{d\rho_0(z)}{dz} = 0, \tag{3}$$

$$\frac{\partial u}{\partial x} + \frac{\partial w}{\partial z} = 0, \tag{4}$$

where $\rho'(x,z,t)$ is the fluctuating part of the density field, $\nu$ the kinematic viscosity, $u$, $w$ the velocity components in the $x$ and $z$ directions and $p$ the pressure. Recognizing that the vertical displacement $\zeta$ is related to the vertical velocity by

$$w = \frac{\partial \zeta}{\partial t},$$

the incompressibility equation may be written as

$$\rho' = \frac{-d\rho_0(z)}{dz}\zeta.$$

This may be used to reduce Eqs. (1)–(4) to

$$\rho_0(z)\left(\frac{\partial u}{\partial t} - \nu\frac{\partial^2 u}{\partial z^2}\right) + \frac{\partial p}{\partial x} = 0, \tag{5}$$

$$g\frac{d\rho_0(z)}{dz}\zeta - \frac{\partial p}{\partial z} = 0, \tag{6}$$

$$\frac{\partial u}{\partial x} + \frac{\partial^2 \zeta}{\partial z \partial t} = 0. \tag{7}$$

Assuming that the Brunt-Väisälä frequency

$$N = \left(-\frac{g}{\rho_0}\frac{d\rho_0(z)}{dz}\right)^{1/2}$$

and the viscosity $\nu$ are constants, and making use of the Boussinesq approximation, Eqs. (5)–(7) may be reduced to a single differential equation in $p$, i.e.,

$$\nu\frac{\partial^5 p}{\partial t \partial^4 z} - \frac{\partial^4 p}{\partial^2 t \partial^2 z} - N^2\frac{\partial^2 p}{\partial x^2} = 0. \tag{8}$$

The condition that $u = 0$ at $x = 0$, $L$ is satisfied by considering standing waves in the $x$ direction:

$$\left.\begin{aligned} u(x,z,t) &= U(z)e^{-i\sigma t}\sin kx \\ p(x,z,t) &= P(z)e^{-i\sigma t}\cos kx \\ \zeta(x,z,t) &= Z(z)e^{-i\sigma t}\cos kx \end{aligned}\right\},$$

where $k = m\pi/L$ and $m$ is the longitudinal modal number. Substitution of the above into Eq. (8) yields

$$is^2 \frac{d^4P(z)}{dz^4} - \frac{d^2P(z)}{dz^2} - \frac{N^2k^2}{\sigma^2} P(z) = 0, \quad (9)$$

where $s^2 \equiv \nu/\sigma$ by definition.

The general solution to Eq. (9) may be written (Ince, 1956, p. 137)

$$P(z) = P_{11} \cos\gamma_1 z + P_{12} \sin\gamma_1 z + P_{21} \cos\gamma_2 z + P_{22} \sin\gamma_2 z, \quad (10)$$

where the $P_{ij}$ are coefficients to be determined from the boundary conditions, and $\gamma_1$ and $\gamma_2$ are the positive roots of the characteristic equation

$$is^2\gamma^4 + \gamma^2 - k^2N^2/\sigma^2 = 0, \quad (11)$$

and are given by

$$\left.\begin{aligned} \gamma_1 &= \left\{\frac{i}{2s^2}\left[1 + \left(1 + \frac{4is^2k^2N^2}{\sigma^2}\right)^{1/2}\right]\right\}^{1/2} \\ \gamma_2 &= \left\{\frac{i}{2s^2}\left[1 - \left(1 + \frac{4is^2k^2N^2}{\sigma^2}\right)^{1/2}\right]\right\}^{1/2} \end{aligned}\right\}.$$

The four boundary conditions needed to solve for $P_{11}$, $P_{12}$, $P_{21}$ and $P_{22}$ are

(i) $\zeta = 0$ or $\partial p/\partial z = 0$ and

(ii) $\partial u/\partial z = \beta u$ at $z = 0$,

(iii) $p = \rho_0 g\zeta$ and

(iv) $\nu\partial u/\partial z = \tau/\rho_0$ at $z = h$,

where the stress conditions (ii) and (iv) along the bottom and free surface, respectively, are added to inviscid conditions (i) and (iii).

For $P(z)$, the conditions (i)–(iv) translate to $P'(0) = 0$, $P'''(0) = \beta P''(0)$, $P'(h) = -N^2P(h)/g$, $P'''(h) = ikN^2\tau/\sigma\nu$, where primes denote order of differentiation. When the wind stress field has spatial scales much larger than the length of the lake, it is expected that the first longitudinal mode is excited most strongly (cf. Mortimer, 1952). The constant wind stress may be Fourier decomposed as follows (the $e^{-i\sigma t}$ factor is implied but omitted):

$$\tau = -|\tau|(4/\pi) \sum_{n=0}^{\infty} (2n + 1)^{-1} \sin[(2n + 1)\pi x/L].$$

In the following analysis we consider response to the first longitudinal forcing mode only ($n = 0$), i.e., we set

$$\tau = -|\tau|(4/\pi) \sin(\pi x/L) = -|\tau| \frac{4}{L} \frac{\sin kx}{k}.$$

We obtain the following system of equations relating $P_{ij}$:

$$\gamma_1 P_{12} + \gamma_2 P_{22} = 0, \quad (12)$$

$$\gamma_1^3 P_{12} + \gamma_2^3 P_{22} = \beta(\gamma_1^2 P_{11} + \gamma_2^2 P_{21}), \quad (13)$$

$$(N^2g^{-1} \cos\gamma_1 h - \gamma_1 \sin\gamma_1 h)P'' + (N^2g^{-1} \cos\gamma_2 h - \gamma_2 \sin\gamma_2 h)P_{21} + (N^2g^{-1} \sin\gamma_1 h + \gamma_1 \cos\gamma_1 h)P_{12} + (N^2g^{-1} \sin\gamma_2 h + \gamma_2 \cos\gamma_2 h)P_{22} = 0, \quad (14)$$

$$\gamma_1^3(-P_{11} \sin\gamma_1 h + P_{12} \cos\gamma_1 h) + \gamma_2^3 \times (-P_{21} \sin\gamma_2 h + P_{22} \cos\gamma_2 h) = -\frac{|\tau|}{is^2} \frac{4}{L} \frac{N^2}{\sigma^2}, \quad (15)$$

which could be solved for the four coefficients. We derive, however, an approximate solution, in which bottom stress is deemed insignificant in comparison with friction within the fluid, i.e., we let $\beta \to 0$ in (13) and conclude that $P_{12}$ and $P_{22}$ become negligible compared to $P_{11}$ and $P_{21}$. Furthermore we anticipate that for the interior solution any change in the free surface elevation is not important and we neglect the terms where $N^2g^{-1}$ appears. This can be justified *a posteriori*.

Using (14) and (15) and taking into account the above simplifications, we derive

$$P(z) = \frac{|\tau|}{is^2} \frac{4}{L} \frac{N^2}{\sigma^2} \frac{1}{\gamma_1^2 - \gamma_2^2}\left(\frac{1}{\gamma_1} \frac{\cos\gamma_1 z}{\sin\gamma_1 h} - \frac{1}{\gamma_2} \frac{\cos\gamma_2 z}{\sin\gamma_2 h}\right), \quad (16)$$

$$U(z) = \frac{|\tau|}{s^2} \frac{4}{\pi} \frac{1}{\rho_0(h)\sigma} \frac{1}{\gamma_1^2 - \gamma_2^2}\left(\frac{\gamma_1 \cos\gamma_1 z}{\sin\gamma_1 h} - \frac{\gamma_2 \cos\gamma_2 z}{\sin\gamma_2 h}\right), \quad (17)$$

$$Z(z) = \frac{|\tau|}{is^2} \frac{4}{L} \frac{1}{\rho_0(h)\sigma^2} \frac{1}{\gamma_1^2 - \gamma_2^2}\left(\frac{\sin\gamma_1 z}{\sin\gamma_1 h} - \frac{\sin\gamma_2 z}{\sin\gamma_2 h}\right). \quad (18)$$

The solutions (16), (17) and (18) reveal two terms in the parentheses, of which the first contains the root $\gamma_1$ and the second the root $\gamma_2$ of the characteristic equation (11). For small viscosity, the expressions for $\gamma_1$ and $\gamma_2$ may be expanded in series and written as

$$\left.\begin{aligned} \gamma_1 &= \left(\frac{i\sigma}{\nu}\right)^{1/2}\left[1 + i\frac{1}{2}\frac{\nu}{\sigma}\frac{k^2N^2}{\sigma^2} + \frac{5}{8}\left(\frac{\nu}{\sigma}\right)^2 \frac{k^4N^4}{\sigma^4} + \ldots\right] \\ \gamma_2 &= \frac{kN}{\sigma}\left[1 - i\frac{1}{2}\frac{\nu}{\sigma}\frac{k^2N^2}{\sigma^2} - \frac{7}{8}\left(\frac{\nu}{\sigma}\right)^2 \frac{k^4N^4}{\sigma^4} + \ldots\right] \end{aligned}\right\}.$$

Thus it is apparent that the term containing $\gamma_1$ is the solution characteristic of a viscous boundary layer, at the surface in this instance, and the term containing $\gamma_2$ is essentially the interior, inviscid solution, modified by viscosity.

Using typical values for the parameters applicable to Lake William, i.e., $L = 3.2 \times 10^3$ m ($k \approx 10^{-3}$ m$^{-1}$), $N = 0.04$ s$^{-1}$, $\nu = (2.0\text{–}10.0) \times 10^{-6}$ m$^2$ s$^{-1}$ (justified later), and considering forcing at the diurnal frequency ($\sigma = 7.27 \times 10^{-5}$ s$^{-1}$) for the first longitudinal mode, we find

$$0.03 < 4 \frac{\nu}{\sigma} \frac{k^2N^2}{\sigma^2} < 0.16$$

and that the above series expansions of $\gamma_1$ and $\gamma_2$ are fully justified.

In the vertical displacement equation (18), the boundary layer term,

$$\frac{\sin\gamma_1 z}{\sin\gamma_1 h} \approx \exp[(1 - i)(\sigma/2\nu)^{1/2}(z - h)]$$

remains small except near the free surface at $z = h$. The boundary layer thickness is of the order of a meter or less.

In the interior of the fluid, the second term in (18) dominates, i.e.,

$$Z_{\text{int}}(z) \approx |\tau| \frac{4}{L} \frac{1}{\rho_0(h)\sigma^2} \frac{\sin\gamma_2 z}{\sin\gamma_2 h}. \qquad (19)$$

Let $\gamma_2 h = n_E \pi$, where $n_E$ is the effective vertical modal number. Then if $n_E$ is an integer, the solution in the inviscid limit corresponds to an exact normal mode of the lake. Using the previously introduced parameters, we find $\gamma_2 = kN/\sigma = 0.54$ m$^{-1}$ and hence $n_E = 2.75$, which shows that at diurnal frequency the response is close to the third normal mode in the vertical. In Fig. 1 the amplitudes of the

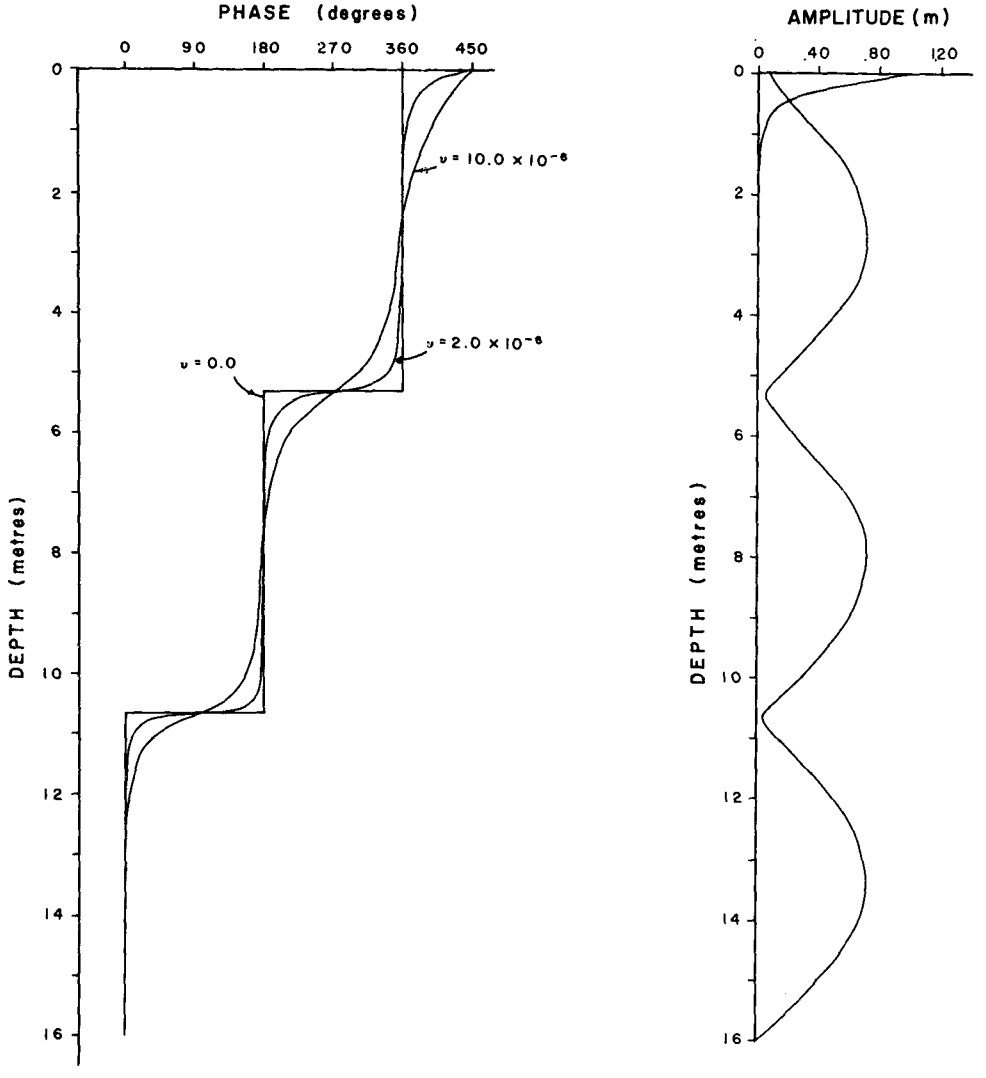


FIG. 1. Phase profiles of the vertical displacement in the third mode for three values of viscosity, and amplitude profiles for the interior and boundary layer solution for $\nu = 5.0 \times 10^{-6}$ m$^2$ s$^{-1}$.

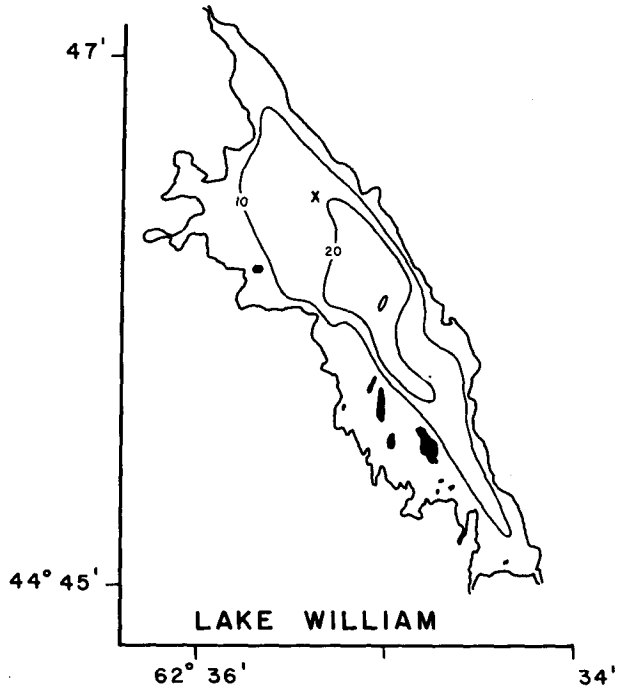


FIG. 2. Outline of Lake William (Nova Scotia) showing the position × of observation and the bathymetry at 10 m intervals.

interior and boundary layer solutions for displacement [the magnitudes of the two terms of Eq. (18), respectively] are shown for $n_E = 3$, i.e., the viscous third mode. The main difference between this and the inviscid third mode is that the amplitude does not vanish at the "nodes". Note that the boundary layer solution in Fig. 1 is drawn on an expanded scale compared to the interior solution. The two curves actually coincide at the surface $z = h$.

The phase profile of the interior solution is given by

$$\phi(z) = \tan^{-1}\left[\mathrm{Im}\left(\frac{\sin\gamma_2 z}{\sin\gamma_2 h}\right)\Big/\mathrm{Re}\left(\frac{\sin\gamma_2 z}{\sin\gamma_2 h}\right)\right].$$

Three profiles of $\phi(z)$ are shown in Fig. 1 for three values of $\nu$. The phase profile corresponding to the inviscid solution concentrates the phase changes at the nodes in an infinitesimally thin layer. As viscosity increases, the phase shift at the nodes becomes smeared out over a finite layer. At molecular values of viscosity ($2.0 \times 10^{-6}$ m$^2$ s$^{-1}$) the phase profile retains the general character of the inviscid profile, but the profile is slightly rounded in the vicinity of the nodes. As the viscosity is increased the phase profile approaches a linear function through the water column, corresponding to the purely progressive wave solution.

Calculation of the vertical energy flux associated with the interior solution (19) shows that it is always directed downward, and thus further confirms that the solution is the physically appropriate one of a system where the only energy source is at the surface. Split into the two progressive wave components, the interior solution consists of a downgoing wave (in energy flow sense) $\propto e^{i\gamma_2 z}$ and the reflected, upward going wave $\propto e^{-i\gamma_2 z}$. At any height above the bottom the amplitude ratio between the two is $\exp[-2\,\mathrm{Im}(\gamma_2 z)]$, and since $\mathrm{Im}\gamma_2 < 0$, the ratio is greater than 1; for example, at $z = h$ and with parameter values as before, the amplitude ratio $= 1.4$ ($\nu = 10.0 \times 10^{-6}$ m$^2$ s$^{-1}$). This means that a wave generated at the surface, by the time it reaches the surface again after being reflected at the bottom, has diminished in amplitude by ~40%. For the third mode the return journey would take three days to complete.

## 3. Data

In this section, temperature time series obtained from a vertical array of thermistors in Lake William, Nova Scotia (Fig. 2), are presented in comparison with some of the theoretical results. The comparisons are naturally restricted, by the techniques of time series analysis, to the most consistent oscillations possessing the largest amplitudes. In the data to be presented, the largest internal displacements are usually found near the diurnal frequency. This, of course, excludes the effects of violent storms, which, for a few hours, are capable of exerting a wind stress at the surface of the lake a thousand times greater than a typical rms stress. Most of the internal motion excited by a storm appears to be involved in changing the potential energy of the stratification rather than initiating persistent internal seiche oscillations of large amplitude.

Using records of 20 days or so, obtained during typical non-stormy summer weather conditions, it shall be demonstrated that the magnitude of the theoretically predicted phase change through the water column agrees with that observed, especially near the diurnal frequency. The shape of the phase profile shall also be shown to possess the smeared characteristics predicted by the viscous theory, thereby confirming that the migrating aspect of the temperature structures may be described as an effect of viscosity. The data were obtained during July 1975 and consists of data from 40 thermistors in a vertical array from 2 to 14 m. The sensor spacing in the array was variable from 0.20 to 0.80 m.

The data were filtered twice; the first filter had a cutoff period of 2 h and was applied to the original data before it was decimated from a 10 min to a 1 h sampling interval. A second filter with a cutoff period of 16 h was applied without decimation to further remove high-frequency energy before plotting.

Spectral analysis was performed on the thermistor

data after the preliminary filtering stage. The hourly wind data, which had been collected at Halifax International Airport, located 12 km northeast of the lake, was subjected to spectral analysis directly.

In Table 1 the wind stress along the long axis of the lake and the vertical displacement at 12.5 m depth in the lake are listed at various frequencies. Vertical displacement is derived from spectral values of temperature fluctuation via the relation

$$D = [\psi(f)\Delta f(dT/dz)^{-2}]^{1/2},$$

where $dT/dz = 0.78°C/m^{-1}$ is the average vertical temperature gradient at that depth, $\psi(f)$ is the temperature spectral energy at frequency $f$ and $\Delta f$ the bandwidth.

The wind stress $\tau$ is calculated by

$$\tau = \rho_a C_D \psi(f)\Delta f,$$

where $\rho_a = 1.2$ kg m$^{-3}$ is the density of air, $C_D = 10^{-3}$ is the drag coefficient and $\psi(f)$ is now the spectral energy of the wind.

In the spectral analysis both the temperature and wind records were divided into seven nonoverlapping blocks of 64 hourly samples each, making the total analyzed record 18.7 days long.

The choice of the 12.5 m temperature record for tabulation was made because it is representative of the signals at the deeper thermistors. The shallower signals tend to have features, such as the seasonal drift, that are caused by heat exchange across the surface rather than by vertical motion in the lake, and have therefore more energy at the low frequencies.

Tabulated values show that whereas wind stress falls off fairly smoothly with frequency, vertical displacement has peaks, most notably in the third and fifth frequency band. The values in the last column give an indication of the vertical motion per unit stress. Maximum values coincide with the displacement peaks, suggesting that the lake absorbs wind energy at some frequencies more efficiently than at others.

The discussion in the preceding section on the response of the lake with the given size and stratification leads us to believe that the increased vertical motion per unit wind stress in the third, fifth and seventh frequency bands is a manifestation of response in the third, second and first vertical mode, respectively. The reason for the third mode possessing the largest displacement is found in two opposing effects along the frequency axis; namely, the vertical response per unit stress is very small at low frequencies (high modes) and increases with frequency to a maximum at the fundamental mode frequency. However, as seen in Table 1, the stress diminishes with frequency, whence the net effect is strongest at approximately the diurnal frequency and the third mode.

In the remaining analysis we concentrate on the strongest response in the diurnal frequency band. The second filter applied to the data effectively removes the signals of frequency higher than the fourth band.

The filtered temperature records from 33 thermistors for the 20 days beginning 7 July 1975 are shown in Fig. 3, accompanied by the hourly wind vector at the Halifax International Airport.

The records shown are spread between the depths 4.9 m at the top of the array to 14.0 m at the bottom. The eight records from above 4.9 m have been omitted because the sensors were in the mixed layer most of the time and the records are essentially identical. The long-term trend of temperature which appears in most of the records of Fig. 3 is a function of depth. Negligible at the bottom sensors, the variation increases up the water column, and at the upper sensors the long-term change is a measure of the seasonal temperature change in the upper mixed layer. Part of the heating in the upper thermocline is presumably due to solar radiation and part to the downward mixing of heat. This slow heating does not appear to significantly affect the internal oscillations during the period of the observations.

The main phenomenon of interest in the tempera-

TABLE 1. Vertical displacement and wind stress and their ratio as a function of frequency.

| Frequency band number | Frequency (cph) | Displacement (m) | Stress × $10^3$ (N m$^{-2}$) | Ratio × $10^{-3}$ (m/N m$^{-2}$) |
|---|---|---|---|---|
| 1 | 0.0135 ± 0.0078 | 0.035 ± 0.007 | 1.03 ± 0.56 | 0.03 |
| 2 | 0.0303 ± 0.0078 | 0.070 ± 0.012 | 0.48 ± 0.27 | 0.15 |
| 3 | 0.0462 ± 0.0078 | 0.140 ± 0.038 | 0.52 ± 0.26 | 0.27 |
| 4 | 0.0620 ± 0.0078 | 0.054 ± 0.012 | 0.27 ± 0.19 | 0.20 |
| 5 | 0.0845 ± 0.0157 | 0.126 ± 0.031 | 0.37 ± 0.17 | 0.34 |
| 6 | 0.116 ± 0.0157 | 0.071 ± 0.02 | 0.26 ± 0.17 | 0.27 |
| 7 | 0.154 ± 0.0234 | 0.087 ± 0.027 | 0.20 ± 0.07 | 0.44 |
| 8 | 0.209 ± 0.0313 | 0.070 ± 0.025 | 0.24 ± 0.12 | 0.29 |
| 9 | 0.279 ± 0.0391 | 0.052 ± 0.004 | 0.25 ± 0.12 | 0.21 |
| 10 | 0.371 ± 0.055 | 0.037 ± 0.004 | 0.28 ± 0.07 | 0.13 |
| 11 | 0.467 ± 0.0391 | 0.024 ± 0.003 | 0.09 ± 0.05 | 0.27 |

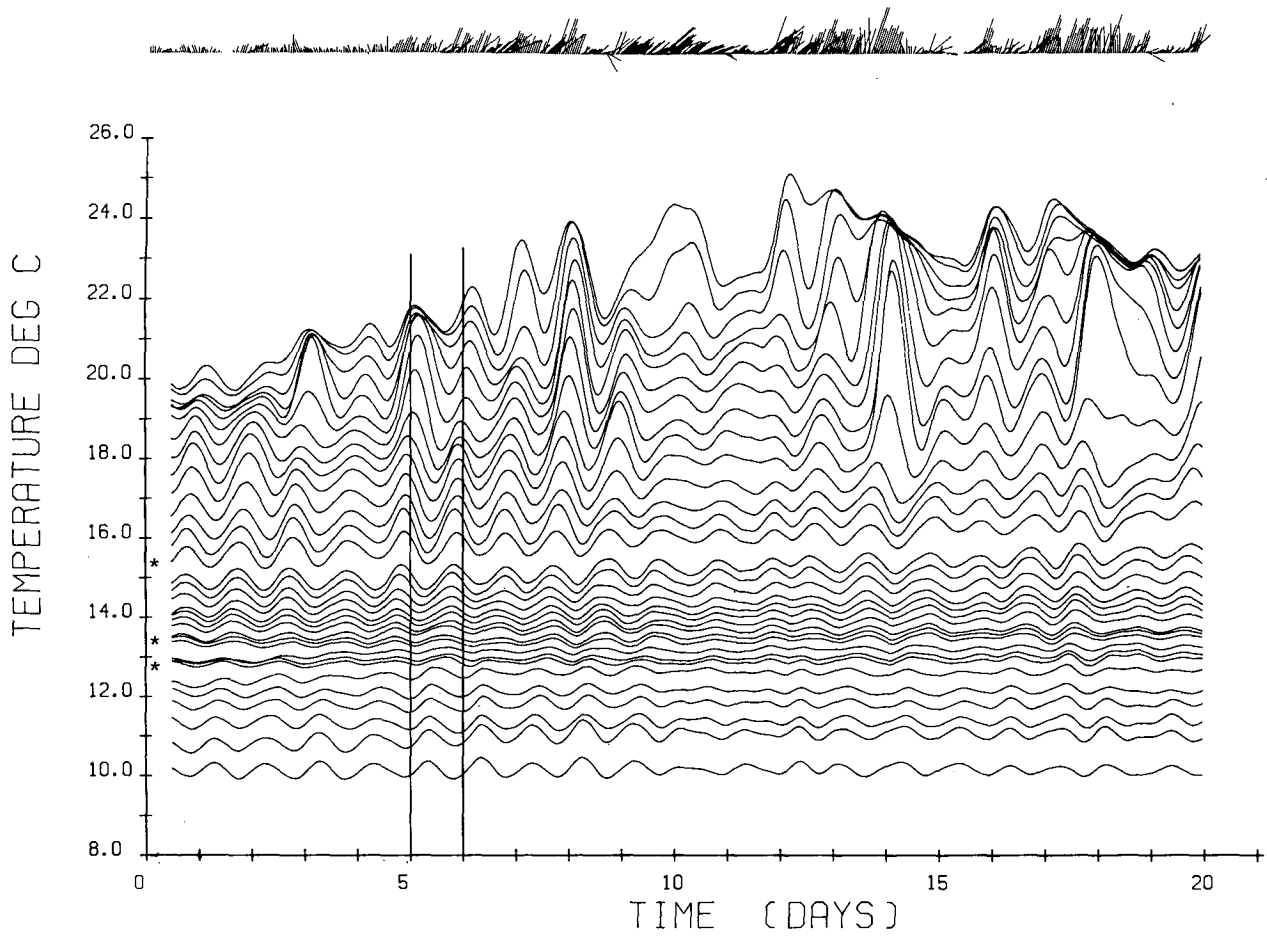


FIG. 3. Temperature versus time at 33 depths for 20 days from 7 July 1975; zero time is 2100 GMT. The records are 0.2 m apart except where an asterisk indicates a missing record and except the bottom six records which are spaced 0.8–0.4 m apart in decreasing steps of 0.1 m from the bottom.

ture time series shown in Fig. 3 is the diurnal oscillation evident at all sensors. The phase of this oscillation, especially from day 1 to 10, clearly varies continuously with depth, with the lower records leading the upper ones. The temperature oscillation near the bottom is almost in phase with that in the upper part of the thermocline, while that near 15°C is nearly 180° out of phase with both the near-surface and near-bottom oscillations. Two vertical lines at the beginning of days 5 and 6 help to emphasize the phase shift of the temperature oscillation and the vertical temperature gradient at two points in time. Regions of low and high vertical gradient are evident where the temperature records are, respectively, close and far apart. These anomalous gradients move vertically through the water column at the same rate as the phase of the oscillation.

The total phase shift across the sensor array appears to be about 360° which strongly suggests the presence of the third normal mode. The previously computed effective mode number of 2.75 implies that there are two nodes between the top and the bottom of the lake. Across each node there should exist a smeared phase shift of 180° making a total phase shift across the thermocline of 360°, which agrees with the visual impression of Fig. 3.

The 5- and 15-day average temperatures were computed for each record and from these averages smooth vertical profiles of density are constructed for each 5- and 15-day interval. The first three nonoverlapping 5-day average profiles are shown in Fig. 4a. The first 15-day average profile is indistinguishable from the average profile for days 6 to 10, i.e., curve b. From the smoothed density profile, estimates of the average vertical density gradient and Brunt-Väisälä frequency $N$ were obtained. The distribution of $N$ with depth based on the first 15-day average density profile is also shown in Fig. 4b. With the vertical distribution of $N$ and the algorithm of Bell (1971) it was possible to calculate the third mode vertical velocity function (Fig. 4b). This calculation determines the positions of the nodes in relation to the stratifica-

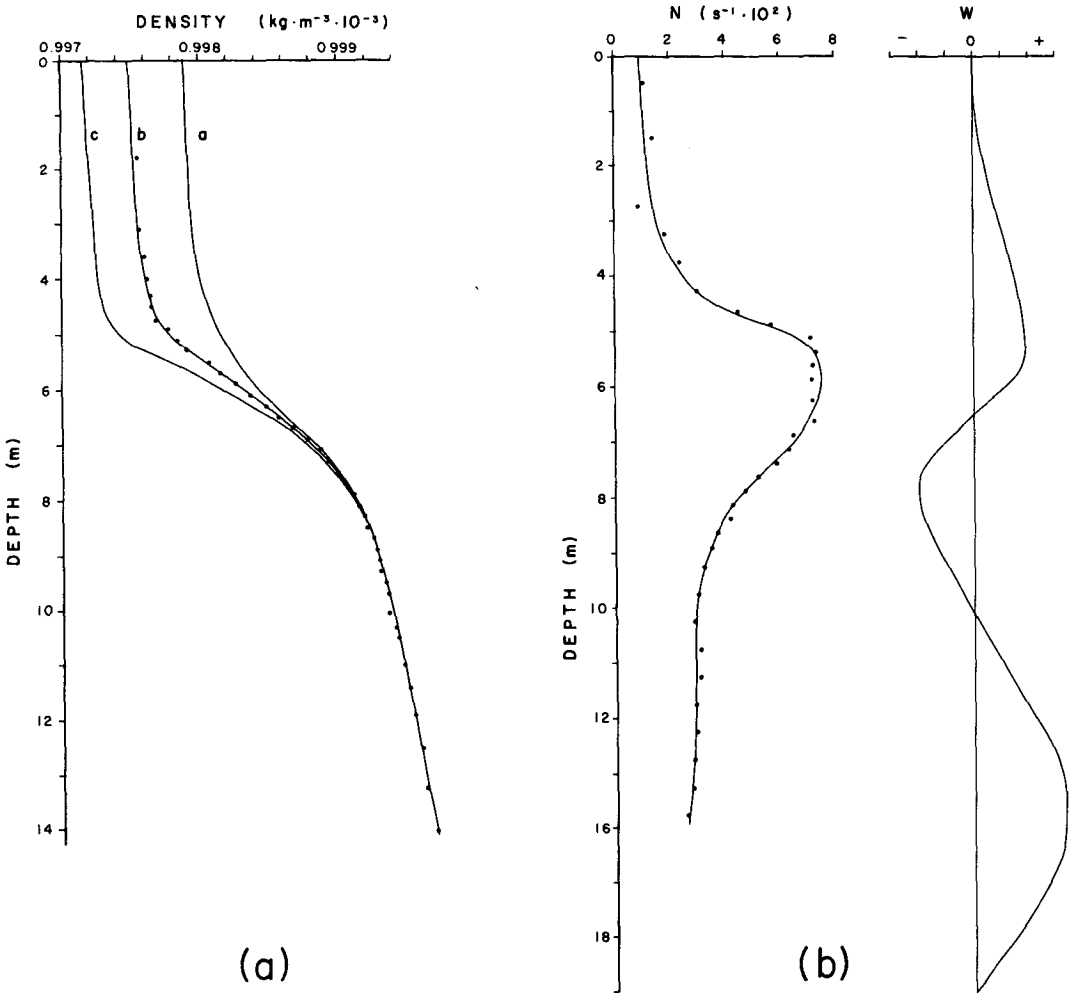


FIG. 4a. The first three (a, b, c respectively) 5-day average density profiles for the data plotted in Fig. 3. The average for the first 15 days is nearly identical with curve b. The data points are only given for the middle period.

FIG. 4b. Profile of Brunt-Väisälä frequency $N$ derived from the average density profile, for the first 15 days of the record and the profile of the vertical velocity $w$ calculated numerically for the inviscid third mode.

tion, and thereby determines the inviscid phase profile. For the weakly viscous case, the nodes of the third mode will be at the same depths as for the inviscid case.

A quantitative assessment of the phase profile from the data of Fig. 3 is obtained from the cross-spectrum statistics between the temperature records. The phase calculations in the diurnal frequency band for the records between 4 and 14 m relative to the sensor at 11.9 m are presented in Fig. 5, and compared with three computed phase profiles. The observed profile shows two regions of relatively rapidly changing phase. These are centered at 6.5 and 10 m corresponding closely to the depths of the nodes of the inviscid third mode as predicted by the numerical calculation (Fig. 4b), the phase of which is shown by the steplike profile in Fig. 5. The other computed phase profiles shown in Fig. 5 are reconstructions of the viscous phase profiles shown in Fig. 1a. Although the viscous phases were computed for a constant $N$, the nodal depths have been adjusted to coincide with those of the inviscid model, which is based on the observed profile of $N$, to facilitate comparison with the measured profile. Near the upper node the theoretical curve for $\nu = 10.0 \times 10^{-6}$ m$^2$ s$^{-1}$ agrees well with the observed curve. The agreement between the measured and predicted phase profile for $\nu = 10.0 \times 10^{-6}$ m$^2$ s$^{-1}$ gives us a good estimate of the true value of viscosity. Larger values would smooth the profile substantially more than observed, the smaller values would show a more steplike structure at the nodes.

At the lower nodal position the temperature records shown in Fig. 3 exhibit a pronounced minimum in amplitude indicating the presence of a

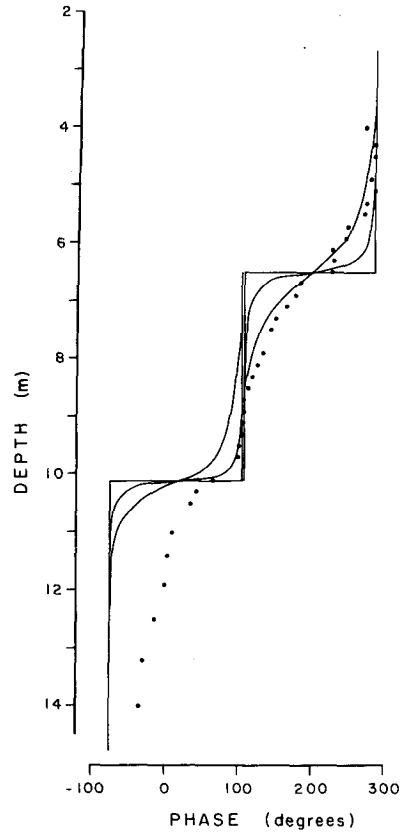


FIG. 5. Observed phase profile for the first 18⅔ days of the 1975 Lake William data in the diurnal frequency band compared to the inviscid phase profile for the third mode. Also shown are two viscous phase profiles taken from Fig. 1a but compressed vertically to make the nodes match those of the inviscid profile.

node in the vertical displacement. No similar decrease in displacement is evident at the expected position of the upper node which should be in the vicinity of 19°C (equivalent to a density of 0.9984 $\times$ $10^3$ kg m$^{-3}$ or a depth of 6 m in Fig. 4a). Calculations of vertical displacement (not shown) confirmed the visual impression in Fig. 3 that there is a decrease in displacement at the lower node between 9 and 10 m, but no apparent decrease at the upper node. At the bottom sensors, the vertical displacement in the frequency band 0.0462 $\pm$ 0.0076 cph is approximately 0.14 m. This decreases to 0.07 m at 9.5 m (13°C) and increases back to 0.15 m at the upper records. These values may be compared with theoretical predictions given by Eq. (19), i.e.,

$$Z_{\text{int}}(z) \approx \frac{|\tau|}{\rho_0(h)} \frac{4}{L} \frac{1}{\sigma^2} \frac{\sin\gamma_2 z}{\sin\gamma_2 h}.$$

Therefore, the magnitude of the displacement is

$$Z_{\text{int}}(z) = \frac{|\tau|}{\rho_0(h)} \frac{4}{L} \frac{1}{\sigma^2} \times \left[ \frac{\sin^2 \frac{kN}{\sigma} z + \sinh^2 \frac{\nu}{2\sigma}\left(\frac{kN}{\sigma}\right)^3 z}{\sin^2 \frac{kN}{\sigma} h + \sinh^2 \frac{\nu}{2\sigma}\left(\frac{kN}{\sigma}\right) h} \right].$$

At the nodal points, $\sin(kN/\sigma)z_{\text{nodes}} = 0$, whereas maximum displacement occurs at antinodes, where $\sin(kN/\sigma)z_{\text{antinodes}} = 1$. For the Lake William parameters ($h$ = 16 m, $L = 3.2 \times 10^3$ m, $N$ = 0.4 s$^{-1}$), we find

$$\sin^2(kNh/\sigma) \sim \tfrac{1}{2} \gg \sinh^2(\nu/2\sigma)(kN/\sigma)k.$$

Therefore, at the nodal points

$$|Z_{\text{int}}|_{\text{nodes}} \approx \frac{|\tau|}{\rho_0(h)} \frac{4}{L} \frac{\sqrt{2}}{\sigma^2} \sinh \frac{\nu}{2\sigma}\left(\frac{kN}{\sigma}\right)^3 z_{\text{nodes}}$$

and similarly at antinodes

$$|Z_{\text{int}}|_{\text{antinodes}} \approx \frac{|\tau|}{\rho_0(h)} \frac{4}{L} \frac{\sqrt{2}}{\sigma^2}.$$

The wind stress at the surface of the lake for the diurnal frequency band from Table 1 is $2.6 \times 10^{-4} < |\tau| < 7.8 \times 10^{-4}$ N m$^{-2}$. With this range in wind stress, the displacement amplitude at *antinodes* is calculated to be

$$0.09 < |Z_{\text{int}}|_{\text{antinodes}} < 0.27 \text{ m}.$$

With $\nu = 10 \times 10^{-6}$ m$^2$ s$^{-1}$, the ratio of displacement amplitude at the nodes to that at the antinodes is $0.063n$ where $n$ = 0, 1, 2, . . . , $< n_E$ is the nodal number ($n$ = 0 at the bottom).

The calculated displacements are in good agreement with measured values away from the nodes, where meaured values tend to be high when compared with theoretical expectations. A choice of higher viscosity would increase the expected values at the nodes, but the evidence from the phase profiles suggests that viscosity is confined to low values within a narrow range. The discrepancies between observations and theory must partly have their origin in features that the simple theory omits, such as the variation of stratification and viscosity in depth and/or in time during the experiment.

The fact that the lower node is more prominent than the upper node in the data indicates to us that dissipation within the body of the water is more important than scattering or viscous effects at the lake bottom. Although phase progression is caused by dissipation anywhere in the system, the ratio of progressive to standing wave depends on where dissipation occurs. If internal friction losses were small compared to bottom effects, the ratio of progressive to standing wave would be essentially the same throughout the depth and the nodes equally prominent. With internal friction dominant, how-

ever, the standing wave component is relatively larger at the lower node, which is therefore more prominent.

## 4. Summary and conclusions

Vertical temperature profiles obtained in two stratified freshwater lakes (Lazier, 1973, 1977) demonstrate the existence of vertically migrating finestructure in the thermocline. The structures represent the distortions of the vertical temperature profile produced by continuous variations with depth of the vertical displacements associated with the internal oscillations of the lake. The migrating aspect of these structures is not consistent with the previously existing inviscid theories of the internal motion in lakes for which the normal modes in a stratified lake exist as pure standing waves, since such theories give a discontinuous phase change of 180° across the nodes of the oscillations and spatially stationary distortions or structures in the vertical temperature profile.

A new theory of the wind-forced internal motion in a long, narrow, nonrotating viscous lake of constant stratification has been developed. The inclusion of weak viscosity in the theory results in a gradual change of phase across the nodes of the vertical displacement profile. This continuous change of phase through the water column allows the theory to model the migrating features that have ben observed in the lakes.

Two aspects of the forced viscous theory have been compared to the data collected with a fixed vertical array of temperature sensors in Lake William. The shape of the observed vertical phase profile for the forced diurnal oscillation in the lake is similar to the profile predicted by the forced viscous theory using a viscosity of about $10.0 \times 10^{-6}$ m$^2$ s$^{-1}$, the range of viscosity being restricted by the shape of the phase profile. Larger values would yield a phase profile nearly linear with depth and smaller values a phase profile with too rapid a change near the nodes, both inconsistent with the data.

The success of the theory in describing the internal motion of a viscous lake and the behavior of the finestructure encourage the application of the theory to oceanic data. The oceanic case does not, however, require an explanation in terms of forced modes of oscillation given in this paper, but is better described in terms of progressive waves which can cause structures which migrate in the same direction as the phase speed of the waves. Possibly a large percentage of the finestructure in the main oceanic thermocline described by Cooper and Stommel (1968) as ubiquitous is due to progressive internal waves of small vertical wavelength. Recently R. A. Clarke (private communication) and N. Oakey and J. A. Elliott (private communication) have independently observed migrating finestructures in time series of temperature and salinity profiles in the ocean. Also Pinkel (1975, Fig. 5) shows some migrating temperature structures in a series of temperature profiles obtained from *FLIP* off the California coast. These structures are similar in appearance to those observed in freshwater, and it is reasonable to expect that they are created by internal waves. The mechanisms which define the vertical and horizontal scales of such structures are unknown, however. It is also often observed that the vertical profile through structures, in both the oceanic and freshwater case, are much sharper than present small-amplitude internal wave theory would predict. More detailed descriptions of the observed structures in terms of internal wave theory will have to deal with such problems.

*Acknowledgments.* We wish to record our gratitude to Messrs. B. D. Carson and S. G. Glazebrook for assistance in the field and to Dr. G. T. Needler for support and useful criticism throughout. We are also indebted to the Nova Scotia Department of Lands and Forests for allowing us the use of their facilities at Lake William.

## REFERENCES

Bell, T. H., 1971: Numerical calculation of dispersion relations for internal gravity waves. Naval Res. Lab. Rep. 7294, Washington, D. C., 44 pp.

Cooper, J. W., and H. Stommel, 1968: Regularly spaced steps in the main thermocline near Bermuda. *J. Geophys. Res.*, **73**, 5814–5854.

Heaps, N. S., 1960: Seiches in a narrow lake, uniformly stratified in three layers. *Geophys. J. Roy. Astron. Soc.*, **5**, 134–156.

Ince, E. L., 1956: *Ordinary Differential Equations*. Dover, 558 pp.

Lazier, J. R. N., 1973: Temporal changes in some fresh water temperature structures. *J. Phys. Oceanogr.*, **3**, 226–229.

——, 1977: An investigation of thermal structure in two fresh water lakes. Ph.D. thesis, University of Southampton, 135 pp.

Mortimer, C. H., 1952: Water movements in lakes during summer stratification; evidence from the distribution of temperature in Windermere. *Phil. Trans. Roy. Soc. London*, **B236**, 355–404.

Mowbray, D. E., and B. S. H. Rarity, 1967: A theoretical and experimental investigation of the phase configuration of internal waves of small amplitude in a density stratified fluid. *J. Fluid Mech.*, **38**, 1–16.

Pinkel, R., 1975: Upper ocean internal wave observations from *FLIP*. *J. Geophys. Res.*, **80**, 3892–3910.

Proudman, J., 1953: *Dynamical Oceanography*. Methuen & Co., 409 pp.

Turner, J. S., 1973: *Buoyancy Effects in Fluids*. Cambridge University Press, 367 pp.

Watson, E. R., 1904: Movements of the waters of Loch Ness as indicated by temperature observations. *Geograph. J.*, **24**, 430–437.

Wedderburn, E. M., 1912: Temperature observations in Loch Earn, with a further contribution to the hydrodynamical theory of the temperature seiche. *Trans. Roy. Soc. Edinburgh*, **48**, 629–695.